COVER SHEET

A X-ray photoelectron spectroscopy study of HDTMAB distribution within organoclays

Hongping He [†,‡], Qin Zhou [†,§], Ray L. Frost [‡], Barry J. Wood [╫], Loc V. Duong [‡], J. Theo Kloprogge [‡,*]

[†] Guangzhou Institute of Geochemistry, Chinese Academy of Sciences, Guangzhou 510640, China

[‡] Inorganic Materials Research Program, School of Physical and Chemical Sciences, Queensland University of Technology, GPO Box 2434, Brisbane, QLD 4001, Australia

[§] Graduate School of the Chinese Academy of Sciences, Beijing 100039, China

[╫] Brisbane Surface Analysis Facility, University of Queensland, Brisbane, QLD 4072, Australia

Abstract

X-ray photoelectron spectroscopy (XPS) in combination with X-ray diffraction (XRD) and high-resolution thermogravimetric analysis (HRTG) has been used to investigate the surfactant distribution within the organoclays prepared at different surfactant concentrations. This study demonstrates that the surfactant distribution within the organoclays depends strongly on the surfactant loadings. In the organoclays prepared at relative low surfactant concentrations, the surfactant cations mainly locate in the clay interlayer whereas the surfactants occupy both the clay interlayer space and the interparticle pores in the organoclays prepared at high surfactant concentrations. The former adopts a lateral arrangement for the intercalated surfactants within the interlayer while the latter has a paraffin arrangement. This can well explain the dramatic surface area and pore volume decrease of organoclays compared to those of starting clays. XPS survey scans show that, at low surfactant concentration (< 1.0 CEC), the ion exchange between Na^+ and $HDTMA^+$ is dominant whereas both cations and ion pairs occur in the organoclays prepared high concentrations (> 1.0CEC). High-resolution XPS spectra show that the modification of clay with surfactants has prominent influences on the binding energies of the atoms in both clays and surfactants, and nitrogen is the most sensitive to the surfactant distribution within the resultant organoclays.

Introduction

Organoclays represent a family of materials with hydrophobic surfaces, synthesized by modifying swelling clays with various surfactants. During the last 50 years, organoclays have attracted great interest in a number of applications, such as adsorbents for organic pollutants[1-4], rheological control agents[5], reinforcing fillers for plastics[6], clay-based nanocomposites[7], and precursors for preparing mesoporous materials[8, 9].

It is well known that the montmorillonite structure has two silicon-oxygen tetrahedral sheets sandwiching an aluminium octahedral sheet, in which an aluminum ion is octahedrally coordinated to four oxygens and two hydroxyls. Due to the isomorphic substitution within the layers (for example, Al^{3+} replaced by Mg^{2+} or Fe^{2+} in the octahedral sheet; Si^{4+} replaced by Al^{3+} in the tetrahedral sheet), the clay layer is negatively charged, which is counterbalanced by the exchangeable cations (e.g. alkali-metal Na^{+} and alkaline-earth-metal Ca^{2+}) in the interlayer. Hydration of the inorganic cations on the exchange sites causes the clay mineral surface to be hydrophilic in nature, resulting in poor affinity of clays with organic materials. Hence, modifying the clay mineral surface with surfactants, to convert the normally hydrophilic silicate surface to an organophilic surface, is a strategic step in the preparation of clay-based materials (e.g. clay-based nanocomposites, clay-based sorbents for organic pollutants)[10].

A large variety of organoclays have been synthesized using different surfactants[1-4,10-12] and their structures have been characterized using various techniques, including X-ray diffraction (XRD)[11,12], Fourier transform infrared spectroscopy (FTIR)[13-15], Raman spectroscopy[16], thermogravimetric measurement (TG)[17-21], magic-angle-spinning nuclear-magnetic-resonance (MAS NMR)[22,23] and transmission electron microscopy (TEM)[24-26]. In these cases, the detailed information about the interlayer structure, the conformation of the intercalated surfactant and thermal stability of the resultant organoclays rather than the surface characteristics was obtained. However, in various applications of organoclays, the surface characteristics of the resultant organoclays is of high importance since the affinity between the organoclays and the matrix depends strongly on the surface characteristics of the organoclays. Unfortunately, the aforementioned techniques provide little information about the surface characteristics of the organoclays.

X-ray photoelectron spectroscopy (XPS) has been demonstrated to be a powerful technique to investigate the surface characteristics of various materials, including clay minerals and related products[27-30]. XPS can provide elemental analysis for essentially the entire periodic table. Because the electrons whose energies are analyzed arise from a depth of no greater than about 2 – 5 nm, the technique is surface-sensitive and suitable to investigate the surface characteristics of clays and the resultant organoclays.

With the increase of applications in various fields, the study of organoclay surface characteristics will attract great interest. Zhu and coworkers[2] proposed that the various sorption mechanisms of organoclays for pollutants might result from the different distributions of surfactant within the organoclays. Recently, our study

demonstrated that washing the organoclays with solvents resulted in the change of surface energy of the resultant organoclays, resulting from the removal of physically adsorbed surfactant[31]. Both of the abovementioned cases suggest that the distribution of surfactant have a significant effect on the surface property of the organoclays and a consequent influence on their applications.

Unfortunately, to date, there is no publication available on XPS of organoclays, which can provide convincing evidence about the distribution of surfactant within organoclays. The objective of this report is to determine the surfactant distribution within the organoclays using XPS, in conjunction with X-ray diffraction (XRD) and high-resolution thermogravimetric analysis (HRTG). This study demonstrates that the distribution of surfactant (in the interlayer space and outside clay layer) depends strongly on the surfactant loading within organoclays and N 1s spectra are most sensitive to the surfactant distribution. This is of high importance to well understand the microstructure of organoclays and for their applications.

Experimental

Materials

Ca-montmorillonite (Ca-Mt) was obtained from Hebei, China. The sample was purified by sedimentation and the <2 μm fraction was collected and dried at 90 °C. The sample was ground through a 200 mesh sieve and sealed in a glass tube for use. Its cation exchange capacity (CEC) is 90.8 meq/100g, determined by NH^{4+} method as described in the literature[32]. Its chemical formula can be expressed as $Ca_{0.19}Mg_{0.06}Na_{0.01}(Si_{3.96}Al_{0.04})(Al_{1.44}Fe_{0.09}Mg_{0.47})O_{10}(OH)_2{\cdot}nH_2O$, calculated from the chemical analysis result. The surfactant used in this study is hexadecyltrimethylammonium bromide (HDTMAB) with a purity of 99%, provided by YuanJu Chem. Co. Ltd., China.

Preparation of $HDTMA^+$ intercalated montmorillonites

Before synthesis of $HDTMA^+$ intercalated montmorillonites, sodium montmorillonite (Na-Mt) was prepared from Ca-Mt as follows: 10 g of the mixture of Ca-Mt and Na_2CO_3 in the ratio of 94:6 was added into 100 ml of deionized water and stirred at 80 °C for 3 h. During the stirring, several drops of HCl were added into the suspension to dissolve the CO_3^{2-}. Na-Mt was collected by centrifugation and washed with deionized water until the solution was free of chloride (titration with $AgNO_3$). The Na-Mt was dried at 105℃, ground through a 200 mesh sieve and kept in a sealed bottle.

The syntheses of $HDTMA^+$ intercalated montmorillonites were performed by the following procedure: 2.5 g of Na-montmorillonite was first dispersed in 300 ml of deionized water and then a desired amount of HDTMAB was slowly added. The concentrations of $HDTMA^+$ varied from 0.5 CEC to 2.5 CEC of montmorillonite. The reaction mixtures were stirred in a water bath for 9 h at 80 ^oC. All products were washed free of bromide anions (titration with $AgNO_3$), dried at 60 ^oC and ground in an agate mortar to pass through a 200 mesh sieve. The $HDTMA^+$ modified

montmorillonite prepared at the concentration of 0.5 CEC was denoted as 0.5CEC-Mt and the others were marked in the same way.

Characterization

X-ray diffraction (XRD) patterns of the samples were recorded between 1.5 and 20° (2θ) at a scanning speed of 2°/min, using Rigaku D/max-1200 diffractometer with Cu *K*α radiation (30 mA and 40 kV).

High-resolution thermogravimetric analysis (HRTG) was performed on a TA Instruments Inc. Q500 thermobalance. Samples were heated from room temperature to 1000 °C at a heating rate of 10 °C/min with a resolution of 6 °C under N_2 atmosphere (80 cm^3/min). Approximately 30 mg of finely ground sample was heated in an open platinum crucible.

The X-ray photoelectron spectroscopy (XPS) analyses were performed on a Kratos AXIS Ultra with a monochromatic Al X-ray source at 150 W. Each analysis started with a survey scan from 0 to 1200 eV with a dwell time of 100 ms, pass energy of 160 eV at steps of 1 eV with 1 sweep. For the high-resolution analysis, the number of sweeps was increased, the pass energy was lowered to 20 eV at steps of 100 meV and the dwell time was changed to 250 ms. Band component analyses were undertaken using using the Jandel 'Peakfit' software package, which enabled the type of fitting function to be selected and allows specific parameters to be fixed or varied accordingly. Band fitting was done using a Lorenz-Gauss cross-product function with the minimum number of component bands used for the fitting process[33].

Results and discussion

X-ray diffraction (XRD)

One well-established method for characterizing clays and organoclays is the use of X-ray diffraction. This technique enables the expansion of the clay to be determined as well as the crystallite size. Figure 1 shows the XRD patterns of montmorillonites and the resultant organoclays. The basal spacing of Na-Mt is 1.24 nm, which is a characteristic d value for Na-montmorillonite. However, after modification with surfactant, the interlayer height of montmorillonite is obviously increased. With an increase of surfactant concentration in the preparation solution, the basal spacings of the resultant organoclays increase in the following order: 1.24 nm (Na-Mt) → 1.48 nm (0.5CEC-Mt) → 1.78 nm (0.7CEC-Mt) → 1.95 nm (1.0CEC-Mt) → 2.23 nm (1.5CEC-Mt) → 3.61 nm (2.0CEC-Mt) → 3.84 nm (2.5CEC-Mt). As is well known, the layer thickness of montmorillonite is ca. 0.97 nm, hence, the interlayer heights of the resultant organoclays are as follows: 0.51 nm (0.5CEC-Mt), 0.81 nm (0.7CEC-Mt), 0.98 nm (1.0CEC-Mt), 1.26 nm (1.5CEC-Mt), 2.64 nm (2.0CEC-Mt) and 2.87 nm (2.5CEC-Mt).

As demonstrated by the author's previous study[12], the shape of a perfectly straight-chain of $HDTMA^+$ looks like a 'nail', where the long alkyl chain is the 'nail-body' and the chain end holding three methyls is the 'nail-head'. Based on the data of van der Waals radius, covalent bond radius and bond angle, the parameters of $HDTMA^+$ were calculated. When the $HDTMA^+$ lies stretched out, the length of the

'nail' is ~2.53 nm, consisting of the 'nail-head' (0.43 nm) and 'nail-body' (2.1 nm). Our calculation result is similar to that in the literature[34]. The height of the $HDTMA^+$ cation will vary with its orientation. When the plane of the zig-zag arrangement of the carbon atoms of $HDTMA^+$ is perpendicular to the plane of the silicate layer, the height of the 'nail-body' is ~0.46 nm and that of the 'nail-head' is ~0.51 nm. However, the heights of 'nail-body' and 'nail-head' are 0.41 nm and 0.67 nm, respectively, when the plane of the zig-zag arrangement of the carbon atoms of $HDTMA^+$ is parallel to the plane of the silicate layer. The interlayer height of 0.5CEC-Mt equals to the height of the 'nail-head' when the plane of the zig-zag arrangement of the carbon atoms of $HDTMA^+$ is perpendicular to the plane of the clay layer. This suggests that a lateral monolayer was adopted in 0.5CEC-Mt. In the case of 0.7CEC-Mt, the interlayer height is similar to two times of the height of 'nail-body' (0.41 nm) when the plane of the zig-zag arrangement of the carbon atoms of $HDTMA^+$ is parallel to the plane of the clay layer, reflecting a lateral bilayer arrangement. The interlayer heights of 0.98 nm in 1.0CEC-Mt and 1.26 nm in 1.5CEC-Mt correspond to a pseudotrilayer arrangement and a paraffin monolayer, respectively, that have been discussed in detail in the literature[11,12]. In 2.0CEC-Mt and 2.5CEC-Mt, the interlayer heights are obviously larger than the length of $HDTMA^+$, indicating a paraffin bilayer arrangement adopted in the two organoclays with different tilt angles[11,12].

Here, it can be understood that there are five different $HDTMA^+$ arrangements adopted within the montmorillonite interlayer space, i.e., lateral monolayer in 0.5CEC-Mt, lateral bilayer in 0.7CEC-Mt, pseudotrilayer in 1.0CEC-Mt, paraffin monolayer in 1.5CEC-Mt and paraffin bilayer in 2.0CEC-Mt and 2.5CEC-Mt, respectively, in agreement with previous experimental and molecular modeling reports[11,12,35-37]. Figure 2 is the schematics of $HDTMA^+$ intercalated montmorillonites with different arrangement models.

XPS characterization

Figure 3 displays the XPS survey scans of HDTMAB, Na-Mt and the representative organoclays (0.7CEC-Mt and 2.5CEC-Mt). The XPS results clearly show that the presences of carbon, nitrogen and bromine in HDTMAB and sodium, aluminum, silicon, oxygen, magnesium and iron in Na-Mt. The XPS result is in an excellent agreement with our chemical analysis result of montmorillonite. In addition, there is a minor amount of oxygen in HDTMAB and carbon in Na-Mt, resulting from adsorbed CO_2[38]. The XPS survey scans show the presence of calcium in Ca-Mt (not shown) whereas in Na-Mt only sodium was observed (Fig. 3), indicating that the preparation of sodium montmorillonite from calcium montmorillonite in this study was successful.

The ratios of the elemental atomic concentrations in montmorillonite and the resultant organoclays are summarized in Table 1, deduced from the corresponding XPS analyses. This calculation clearly shows that the content of surfactant within the organoclays increases in the order of 0.5CEC-Mt → 0.7CEC-Mt → 1.0CEC-Mt → 1.5CEC-Mt → 2.0CEC-Mt → 2.5CEC-Mt. This is in accordance with our previous studies using other techniques and the reports in the literature[11-25]. Meanwhile, the

Al/Si ratio deduced from the XPS analysis (0.36) is in good agreement with the chemical analysis (0.37). However, the Al/Si ratio in the resultant organoclays decreases with the intercalation of surfactant as shown in Table 1. This results from the increase of the interlayer distance with the intercalation of surfactant, which leads to a decreasing possibility for detecting the Al-O(OH) octahedral sheets sandwiched between the two Si-O tetrahedral sheets of the montmorillonite.

In the XPS survey scans of the resultant organoclays, prominent peaks corresponding to magnesium and a trace to iron are always recorded whereas that of sodium disappears. This reflects that both magnesium and iron are in the montmorillonite structure rather than in the interlayer. This is in agreement with our formula calculation. Meanwhile, the disappearance of the peak corresponding to sodium results from the exchange of sodium ions by surfactant cations.

Interestingly, there is no peak corresponding to bromine recorded in the XPS survey scans of 0.5CEC-Mt, 0.7CEC-Mt and 1.0CEC-Mt whereas it is recorded in the XPS scans of 1.5CEC-Mt, 2.0CEC-Mt and 2.5CEC-Mt. The surfactant contents (in term of CEC) in the resultant organoclays, deduced from the thermogravimetric measurements (not shown), are shown in Table 1. Our calculation indicates that there is more than one CEC of surfactant in 1.5CEC-Mt, 2.0CEC-Mt and 2.5CEC-Mt. Here, it can be understood that, at relative low surfactant concentration ($\leq$ 1 CEC in the present case), the intercalation is dominant and the surfactants enter into the clay interlayer space as cations. On the other hand, the surfactants exist within the organoclays in both formats of cations and molecules when the loaded surfactants are more than 1 CEC[39]. This concept is further supported by the high-resolution XPS scans.

High-resolution XPS

C 1s spectra

The C 1s spectrum of HDTMAB is characterized by two transitions centered at 284.7 and 285.7 eV, corresponding to the C-C bond in the long chain and C-N, respectively (Fig. 4). The C 1s spectra of organoclays show a significant broadening with slight changes in binding energy, indicating more than one type of surfactant-clay interaction. The change trends of binding energy for C-C and C-N as function of CEC are different as shown in Figure 5. For the spectra corresponding to C-C, there is a significant binding energy decrease from HDTMAB to 0.5CEC-Mt and the binding energies for 0.7CEC-Mt and 1.0CEC-Mt are similar to that of 0.5CEC-Mt. However, there is a significant increase from 1.0CEC-Mt to 1.5CEC-Mt, then to 2.0CEC-Mt and finally to 2.5CEC-Mt. The C 1s binding energies of 2.0CEC-Mt and 2.5CEC-Mt are higher than that of HDTMAB. However, the C 1s binding energies of the resultant organoclays, corresponding to the C-N bond, are similar. Here, the C 1s spectra of organoclays show that the local molecular environment of the surfactant has a prominent effect on the binding energy. Molecular modeling[35-37] demonstrates that in all arrangements of surfactant within the clay interlayer, the headgroups (nitrogen) of the alkyl chains will be close to the clay surface due to the strong electrostatic interaction between the negative clay surface

and the positive headgroups of the alkyl chains. This can well explain the similar binding energy of C 1s in C-N for the organoclays with different surfactant arrangements.

Previous reports[13-16,35-37] have shown that, in the organoclays with lower surfactant packing density, the alkyl chains within the interlayer space are parallel within the interlayer space and are individually separated. In this case, the repulsive interaction between the hydrocarbon chain ─ silicate surface is dominant whereas the interaction among the hydrocarbon chains is very weak. The local environment of the intercalated surfactant is absolutely different from those in bulk state. With the increase of surfactant packing density, the interchain interaction among the surfactants becomes the dominant force and the orientation of the hydrocarbon tail changes from parallel to the silicate surface within the interlayer space to parallel but at an angle to the silicate surface as shown by XRD and FTIR results[11-15]. The interaction among alkyl chains will increase with the increase of the surfactant packing density[11,12,21] and this will result in the ordered packing of the alkyl chains as indicated by FTIR and Raman spectroscopy[13-16]. The local environment of the surfactant within the resultant organoclays strongly depends on their loaded amounts, resulting in a variation of the C 1s binding energy associated with the C-C bond in the alkyl chains.

N 1s spectra

The high resolution scans of nitrogen in HDTMAB and the representative organoclays are displayed in Figure 4. For HDTMAB, a single 1s transition is observed with a binding energy of 401.9 eV, which is similar to that reported in a previous study[41]. The high resolution scans of nitrogen in 0.5CEC-Mt, 0.7CEC-Mt and 1.0CEC-Mt show a single 1s transition with a slight increase of the binding energy (ca. 0.4 eV) and full-width-at-half-maximum (FWHM), indicating the local environment of the intercalated surfactant is different from that in bulk state. This is in accordance with the conclusion deduced from the C 1s spectra.

However, the nitrogen high resolution scans of 1.5CEC-Mt, 2.0CEC-Mt and 2.5CEC-Mt show two overlapping bands related to two different N 1s transitions with binding energies of ca. 402.1 and 402.5 eV, respectively. This reflects two different local environments for the surfactant within the resultant organoclays. The later, with a bonding energy (402.5 eV) similar to that in 0.5CEC-Mt, 0.7CEC-Mt and 1.0CEC-Mt, should be attributed to the intercalated surfactant while the former, with a binding energy (402.1 eV) similar to that in bulk HDTMAB, should be attributed to the surfactant outside the clay layers. The ratios of the surfactant outside the clay layers and within the interlayer space are 19:81 in 1.5CEC-Mt, 46:54 in 2.0CEC-Mt and 47:53 in 2.5CEC-Mt, respectively, indicating an increase of the surfactant amount located outside the clay layers with the increase of surfactant loadings as shown by TG analyses.

The nitrogen adsorption-desorption isotherms of Na-Mt and the resultant organoclays show that there are “ink-bottle” like pores in these clays, which could be described as a “house of cards” structure[41,42]. In this case, it is believed that the

surfactants outside the clay layers actually occupy the interparticle pores. This can well explain the dramatic decrease of pore volume and BET surface area of the resultant organoclays with an increase of surfactant loadings (See Supporting Information).

Br 3d spectra

As indicated by the survey scans of the resultant organoclays (Fig. 3), a very weak Br 3d transition begins to occur in the XPS spectrum of 1.5CEC-Mt. The intensity of the Br 3d transition obviously increases in the spectra of 2.0CEC-Mt and 2.5CEC-Mt. Figure 6 displays the high resolution Br 3d scans of HDTMAB, 2.0CEC-Mt and 2.5CEC-Mt.

The Br 3d spectrum of HDTMAB displays two well-resolved transitions centered at 67.1 and 68.2 eV, corresponding to Br $3d_5$ and $3d_3$, respectively. In comparison to the XPS spectrum of HDTMAB, both 2.0CEC-Mt and 2.5CEC-Mt show a broad peak with low intensity and poor resolution for the two transitions. This reflects that the content of bromine in the organoclays is limited and disordered, and ion exchange between $HDTMA^+$ and interlayer cations (Na^+) is dominant[39].

O 1s and Si 2p spectra

The high-resolution O 1s scan of Na-Mt and the simulated curves (Fig. 7a) show that it is difficult to distinguish O and OH in montmorillonite. This is different from the previous study about basic aluminum sulphate and basic aluminum nitrate, in which O and OH in the corresponding materials were clearly identified[33]. There is a small amount of water (ca. 2.39%) remaining in Na-Mt after exposure to ultra high vacuum (10^{-9} – 10^{-10} Torr), as shown by the simulated curves (Fig. 7a). The oxygen in motmorillonite structural sheets corresponds to a binding energy of 532.1 eV while that in water is ca. 535.0 eV. These values are in accord with those reported in the literature[33,43]. However, the high-resolution O 1s scans of the resultant organoclays (Fig. 7) do not show any transition corresponding to H_2O, resulting from the hydrophobicity of the organoclays and high vacuum (10^{-9} Torr) in the detection chamber. Compared to Na-Mt, it can be seen that there is a slight decrease (ca. 1 eV) of the O 1s binding energy in the organoclays. The binding energy change of Si 2p transition from Na-Mt to the resultant organoclays is similar to that of O 1s (Fig. 7 d-f). The binding energy of Si 2p in Na-Mt is 103.0 eV while that for the resultant organoclays increases to 101.9 eV, with a decrease of 1.1 eV. Both the decreases of O 1s and Si 2p binding energies result from the change of the interlayer environment. This is in agreement with the proposal deduced from MAS NMR study of organoclays, which indicates that modifying clays with surfactant results in a measurable shielding of ^{29}Si nuclei in clays[44].

During the intercalation, the prominent change for montmorillonite is that the exchangeable interlayer hydrated cations are replaced by the surfactant cations. As shown by the O 1s XPS spectrum (Fig. 7a), there is a minor amount of H_2O in Na-Mt, corresponding to the strongly bound water of the interlayer cations rather than the surface adsorbed water[45,46]. This part of water links to the oxygen on the clay surface

(Si-O tetrahedral sheet) through hydrogen bond[47,48]. After the interlayer hydrated cations are replaced by the intercalated surfactant, the main interaction between the clay and surfactant includes both the electrostatic attract between the positively charged headgroups (nitrogen) of the alkyl chains and the negatively charged clay surfaces, and a repulsive force between alkyl chain and clay surface as demonstrated by molecular modeling[35-37].

On the basis of abovementioned experimental results, the schematics for the structural evolution from Na-Mt to the resultant organoclays are built as shown in Figure 8. Obviously, two basic organoclay types are formed when modifying clay with surfactant due to the different surfactant distributions: 1) the surfactant mainly occupies the clay interlayer and 2) both the clay interlayer space and external surface are modified by surfactant. Our recent sorption experiments indicate that both surface sorption and partition are involved in the sorption mechanisms for 0.5CEC-Mt, 0.7CEC-Mt and 1.0CEC-Mt to p-nitrophenol whereas partition is dominant for 1.5CEC-Mt, 2.0CEC-Mt and 2.5CEC-Mt (See supporting information). This is a convincing evidence supporting our assumption of the surfactant distribution within organoclays.

Conclusions

In this study, a series of organoclays with different surfactant arrangements within the clay interlayer were prepared. The surfactant distribution within the resultant organoclays was investigated by XPS in combination with XRD and HRTG. In the organoclays prepared at relative low surfactant concentrations (< 1.0CEC), the surfactant cations mainly occupy the clay interlayer with lateral arrangements (lateral monolayer, lateral bilayer and pseudotrilayer). However, when the surfactant concentrations are higher than 1.0CEC, the surfactants occupy both the clay interlayer space and the interparticle pores and paraffin type arrangements of surfactants (paraffin monolayer and paraffin bilayer) are adopted in the clay interlayer spaces. This gives excellent explanations about the dramatic surface area and pore volume decrease of organoclays and different sorption mechanisms (surface sorption and partition) involved in organoclay sorption experiments as reported in the literature.

XPS survey scans show that the peaks corresponding to magnesium and iron are identical in all samples, reflecting these atoms in montmorillonite structure rather in the interlayer or impurities. The peaks corresponding to bromine only appear in the organoclays prepared at high surfactant concentrations (> 1.0CEC). This suggests that both surfactant cations and ion pairs occur in these organoclays, corresponding different interactions between surfactants and clays. The former relates with ion exchange and the latter with sorption.

Generally, modifying clays with surfactants results in a decrease of binding energy of atoms in both clays and surfactants and broadening of the peaks. However, with the increase of surfactant loadings, the FWHM of the related peaks decreases, suggesting the organoclay structure becomes more ordered. This study shows that nitrogen is the most sensitive to the surfactant distribution within the resultant organoclays and the C 1s binding energy of C-C bond in alkyl chain is sensitive to the

local environment of surfactants in organoclays with different arrangements.

Acknowledgments

The financial and infra-structural support from the National Natural Science Foundation of China (Grant No. 40372029), the Inorganic Materials Research Program, Queensland University of Technology and Guangzhou Institute of Geochemistry (International Cooperation Research Program) are gratefully acknowledged.

References

(1) Stackmeyer, M. R. *Appl. Clay Sci.* **1991**, *6*, 39-57.

(2) Meier, L. P.; Nueesch, R.; Madsen, F. T. *J. Colloid Interface Sci.* **2001**, *238*, 24-32.

(3) Zhu, L. Z.; Chen, B. L. *Environ. Sci. Technol.* **2000**, *34*, 2997-3002.

(4) Zhu, L. Z.; Chen, B. L.; Shen, X. Y. *Environ. Sci. Technol.* **2000**, *34*, 468-475.

(5) Manias, E.; Hadziioannou, G.; Brinke, G. *Langmuir* **1996**, *12*, 4587-4593.

(6) Wang, Z.; Pinnavaia, T. J. *Chem. Mater.* **1998**, *10*, 3769-3771.

(7) Ray, S. S.; Okamoto, *Prog. Polym. Sci.* **2003**, *28*, 1539-1641.

(8) Nakatsuji, M.; Ishii, R.; Wang, Z. M.; Ooi, K. *J. Colloid Interface Sci.* **2004**, *272*, 158-166.

(9) Ishii, R.; Nakatsuji, M.; Ooi, K. *Micropor. Mesopor. Mater.* **2005**, *79*, 111-119.

(10) Bergaya, F.; Lagaly, G. *Appl. Clay Sci.* **2001**, *19*, 1-6.

(11) Lagaly, G. *Clay Miner.* **1981**, *16*, 1-21.

(12) Zhu, J. X.; He, H. P.; Guo, J. G.; Yang, D.; Xie, X. D. *Chinese Sci. Bull.* **2003**, *48*, 368-372.

(13) Vaia, R. A.; Teukolsky, R. K.; Giannelis, E. P. *Chem. Mater.* **1994**, *6*, 1017-1022.

(14) Li, Y. Q.; Ishida H. *Langmuir* **2003**, *19*, 2479-2484.

(15) He, H. P.; Frost, R. L.; Zhu, J. X. *Spectrochim Acta A* **2004**, *60*, 2853-2859.

(16) He, H. P.; Frost, R. L.; Xi, Y. F.; Zhu, J. X. *J. Raman Spectros.* **2004**, *35*, 316-323.

(17) Li, Y. Q.; Ishida, H. *Chem. Mater.* **2002**, *14*, 1398-1404.

(18) Xie, W.; Gao, Z. M.; Pan, W. P.; Hunter, D.; Singh, A.; Vaia, R. *Chem. Mater.* **2001**, *13*, 2979-2990.

(19) Xie, W.; Xie, R. C.; Pan, W. P.; Hunter, D.; Koene, B.; Tan, L. S.; Vaia, R. *Chem. Mater.* **2002**, *14*, 4837-4845.

(20) Yariv, S. *Appl. Clay Sci.* **2004**, *24*, 225-236.

(21) He, H. P.; Ding, Z.; Zhu, J. X.; Yuan, P.; Xi, Y. F.; Yang, D.; Frost, R. L. *Clays Clay Miner.* **2005**, *53*, 287-293.

(22) He, H. P.; Frost, R. L.; Deng, F.; Zhu, J. X.; Weng, X. Y.; Yuan, P. *Clays Clay Miner.* **2004**, *52*, 350-356.

(23) Zhu, J. X.; He, H. P.; Zhu, L. Z.; Weng, X. Y.; Deng, F.. *J. Colloid Interface Sci.* **2005**, *286*, 239-244.

(24) Lee, S. Y.; Kim, S. J. *Colloid Surface A* **2002**, *211*, 19-26.

(25) Lee, S. Y.; Kim, S. J. *Clays Clay Miner.* **2002**, *50*, 435-445.

(26) Dana, Y. M.; Yona, C.; Shlomo, N.; Rene, P. *Environ. Sci. Technol.* **2005**, *29*, 1231-1238.

(27) Wittberg, T. N.; Wang, P. S. *Surf. Interface Anal.* **1999**, *27*, 936-940.

(28) Parthasarathy, G.; Choudary, B. M.; Sreedhar, B.; Kunwar, A. C.; Srinivasa, R. *Am. Mineral.* **2003**, *88*, 1983-1988.

(29) Du, J. X.; Zhu, J.; Wilkie, C. A.; Wang, J. Q. *Polym. Degrad. Stabil.* **2002**, *77*, 377-381.

(30) Bueno, M.; Astruc, A.; Lambert, J.; Astruc, M.; Behra, P. *Environ. Sci. Technol.* **2001**, *35*, 1411-1419.

(31) He, H. P.; Duchet, J.; Galy, J.; Gérard, J. F. *J. Colloid Interface Sci.* **2005**.(in press)

(32) He, H. P.; Guo, J. G.; Xie, X. D.; Pen, J. L. *Environ. Int.* **2001**, *26*, 347-352.

(33) Duong, L. V.; Wood, B. J.; Kloprogge, J. T. *Mater. Lett.* **2005**, *59*, 1932-1936.

(34) Yui, T.; Yoshida, H.; Tachibana, H.; Tryk, D. A.; Inoue, H. *Langmuir* **2002**, *18*, 891-896.

(35) Čapková, P.; Burda, J. V.; Weiss, Z.; Schenk, H. *J. Mol. Model.* **1999**, *5*, 8-16.

(36) Zeng, Q. H.; Yu, A. B.; Lu, G. Q.; Standish, R. K. *J. Phys. Chem. B* **2004**, *108*, 10025-10033.

(37) He, H. P.; Galy, J.; Gerard, J. F. *J. Phys. Chem. B.* **2005**, *109*, 13301-13306.

(38) Bugyi, L.; Oszkó, A.; Solymosi, F. *Surf. Sci.* **2000**, *461*, 177-190.
(39) Klapyta, Z.; Fujita, T.; Iyi, N. *Appl. Clay Sci.* **2001**, *19*, 5-10.
(40) Buckley, A. N.; Kelly, M. D.; Nelson, P. F.; Riley, K. W. *Fuel Process. Technol.* **1995**, *43*, 47-60.
(41) Lagaly, G.; Ziesmer, S. *Adv. Colloid Interf.* **2003**, *100*, 105-128.
(42) Burgentzlé, D.; Duchet, J.; Gérard, J. F.; Jupin, A.; Fillon, B. *J. Colloid Interface Sci.* **2004**, *278*, 26-39.
(43) Barr, T. L.; Lishka, M. A. *J. Am. Chem. Soc.* **1986**, *108*, 3178-3186.
(44) Breakwell, I. K.; Homer, J.; Lawrence, M. A. M.; Mcwhinnie, W. R. *Polyhedron*, **1995**, *14*, 2511-2518.
(45) Koster van Groos, A. F.; Guggenheim, S. *Am. Mineral.* **1987**, *72*, 292-298.
(46) Xi, Y. F.; Frost, R. L.; He, H. P.; Kloprogge, J. T.; Bostrom, T. *Langmuir* **2005**, *21*, 8675-8680.
(47) Yan, L.; Roth, C. B.; Low, P. F. *Langmuir* **1996**, *12*, 4421-4429.
(48) Yan, L.; Low, P. F.; Roth, C. B. *Clay Clay Miner.* **1996**, *44*, 749-756.

Table 1 Surfactant loadings and the ratios of atomic concentrations in montmorillonite and the resultant organoclays based on TG and XPS analyses.

Sample	Na-Mt	0.5CEC-Mt	0.7CEC-Mt	1.0CEC-Mt	1.5CEC-Mt	2.0CEC-Mt	2.5CEC-Mt
[a] SL (%)	-	9.73	16.73	22.13	28.19	38.73	44.17
[b] SL (vs CEC)	-	0.33	0.61	0.86	1.19	1.9	2.4
[c] C/Si	-	2.08	2.28	2.69	3.41	5.79	6.58
[d] Al/Si	0.36	0.34	0.32	0.33	0.33	0.28	0.30

a: surfactant loading within the corresponding organoclay, evaluated from high-resolution thermogravimetric analysis.

b: surfactant loading expressed in CEC of montmorillonite (100 g).

c: the ratios of carbon and silicon atomic concentrations in the organoclays.

d: the ratios of aluminun and silicon atomic concentrations in Na-montmorillonite and the organoclays..

Figure Captions

Figure 1 XRD patterns of montmorillonite and the resultant organoclays.

Figure 2 The schematics of organoclays with different arrangements.
a: lateral monolayer; b: lateral bilayer; c: pseudotrilayer;
d: paraffin monolayer; e: paraffin bilayer.

Figure 3 XPS survey scans of HDTMAB, Ca-Mt, Na-Mt and the representative organoclays.

Figure 4 C 1s and N 1s high resolution XPS spectra of HDTMAB and the representative organoclays.
solid line: experimental curve; dot line: deconvolution curve; dash line: fitting curve.

Figure 5 The C 1s binding energy change of C-C and C-N in the resultant organoclays.

Figure 6 Br 3d high resolution XPS spectra of HDTMAB, 2.0CEC-Mt and 2.5CEC-Mt.
solid line: experimental curve; dot line: deconvolution curve; dash line: fitting curve.

Figure 7 O 1s and Si 2p high resolution XPS spectra of Na-Mt and the representative organoclays.
solid line: experimental curve; dot line: deconvolution curve; dash line: fitting curve.

Figure 8 The schematics of Na-Mt and the resultant organoclays.

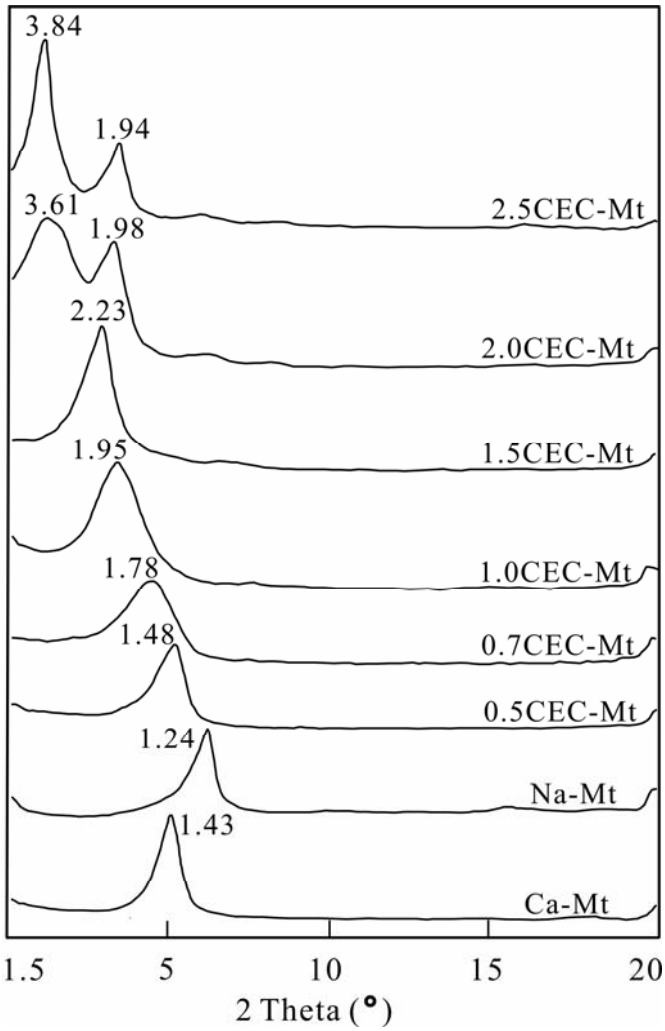

Figure 1 XRD patterns of montmorillonite and the resultant organoclays.

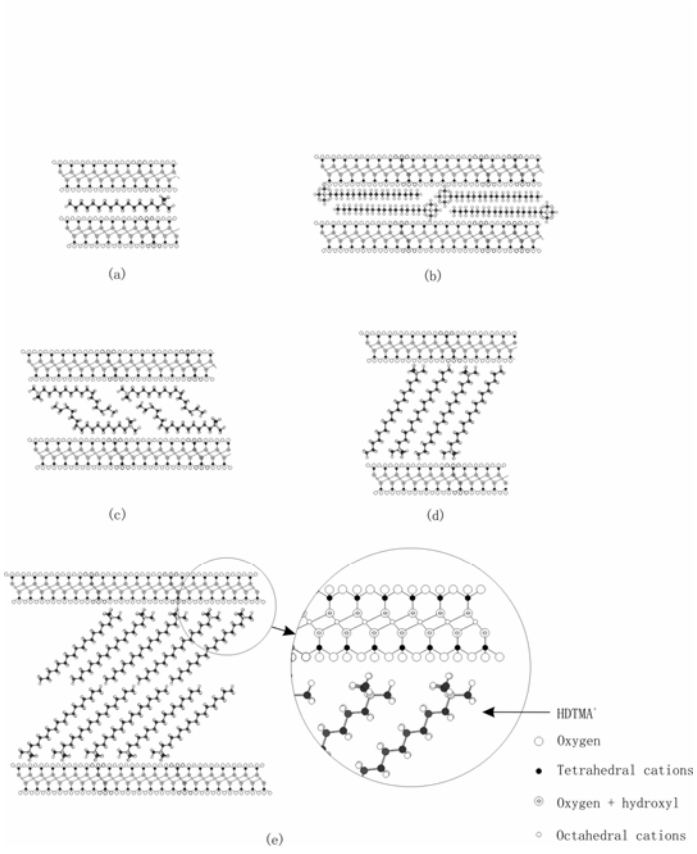

Figure 2 The schematics of organoclays with different arrangements. a: lateral monolayer; b: lateral bilayer; c: pseudotrilayer; d: paraffin monolayer; e: paraffin bilayer.

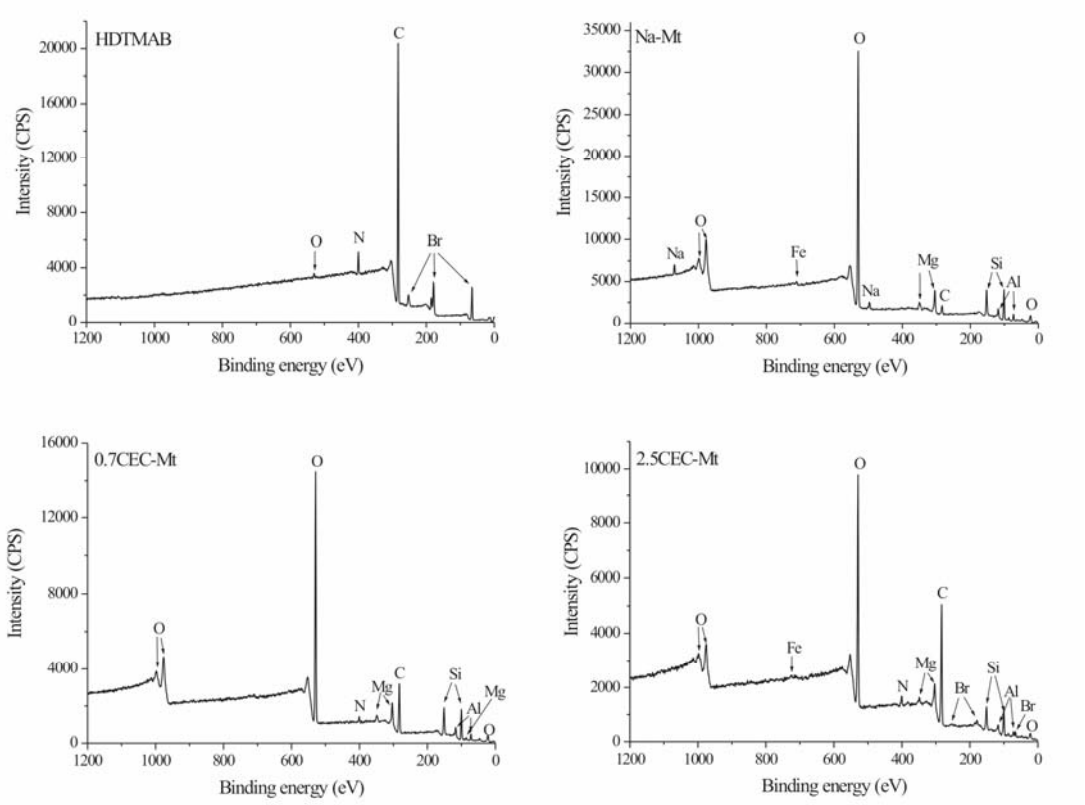

Figure 3 XPS survey scans of HDTMAB, Na-Mt and the representative organoclays.

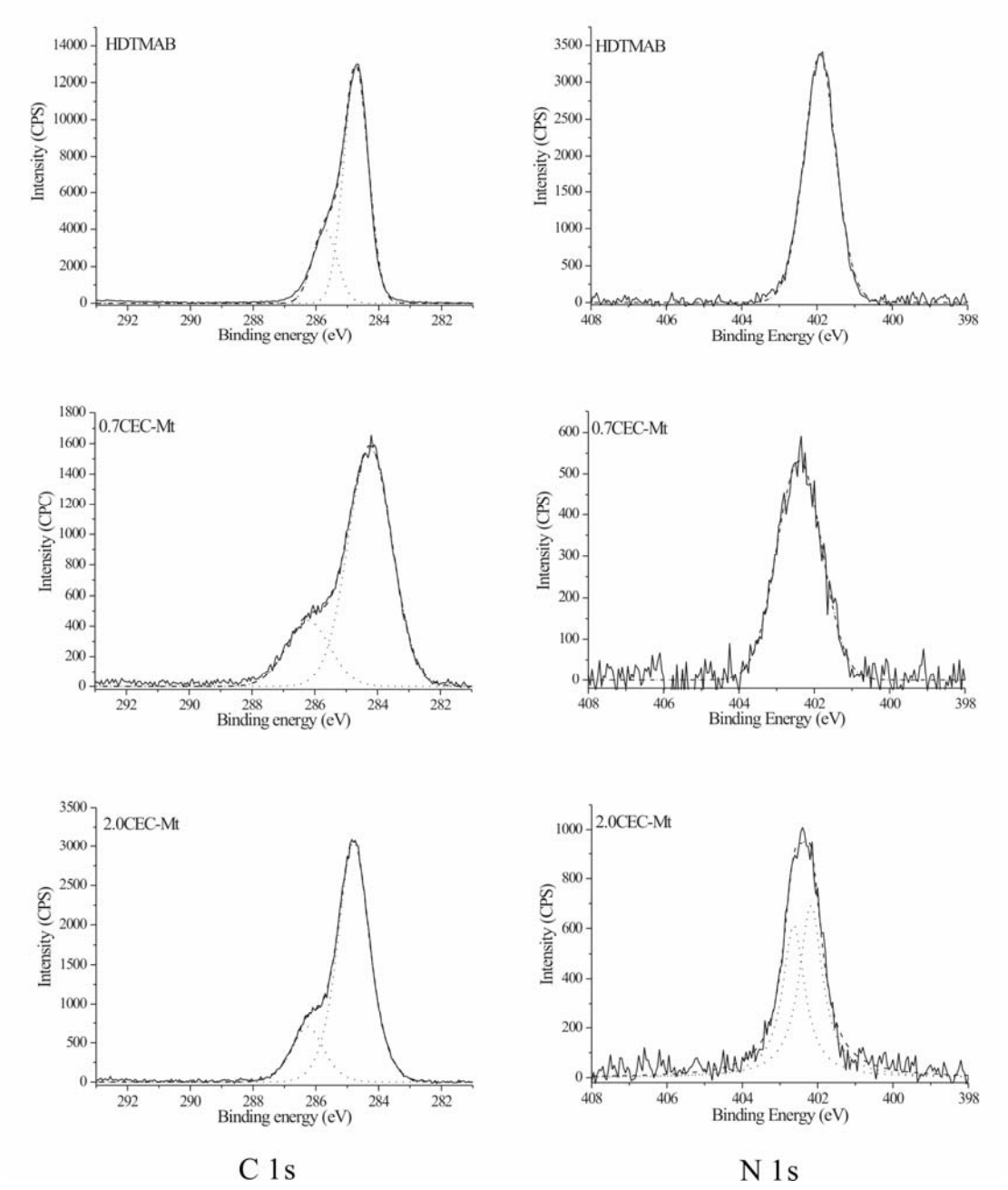

Figure 4 C 1s and N 1s high resolution XPS spectra of HDTMAB and the representative organoclays. solid line: experimental curve; dot line: deconvolution curve; dash line: fitting curve.

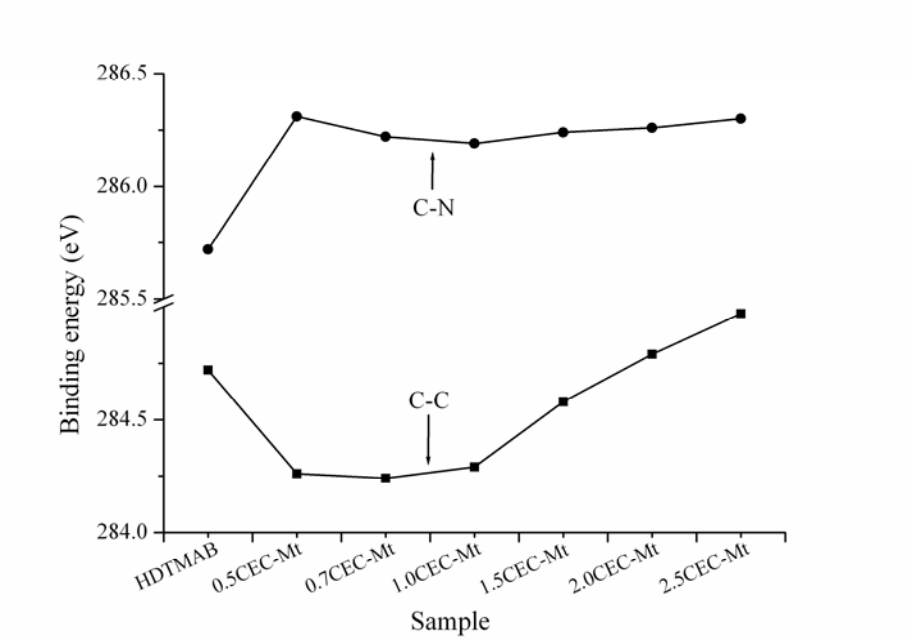

Figure 5 The C 1s binding energy change of C-C and C-N in the resultant organoclays.

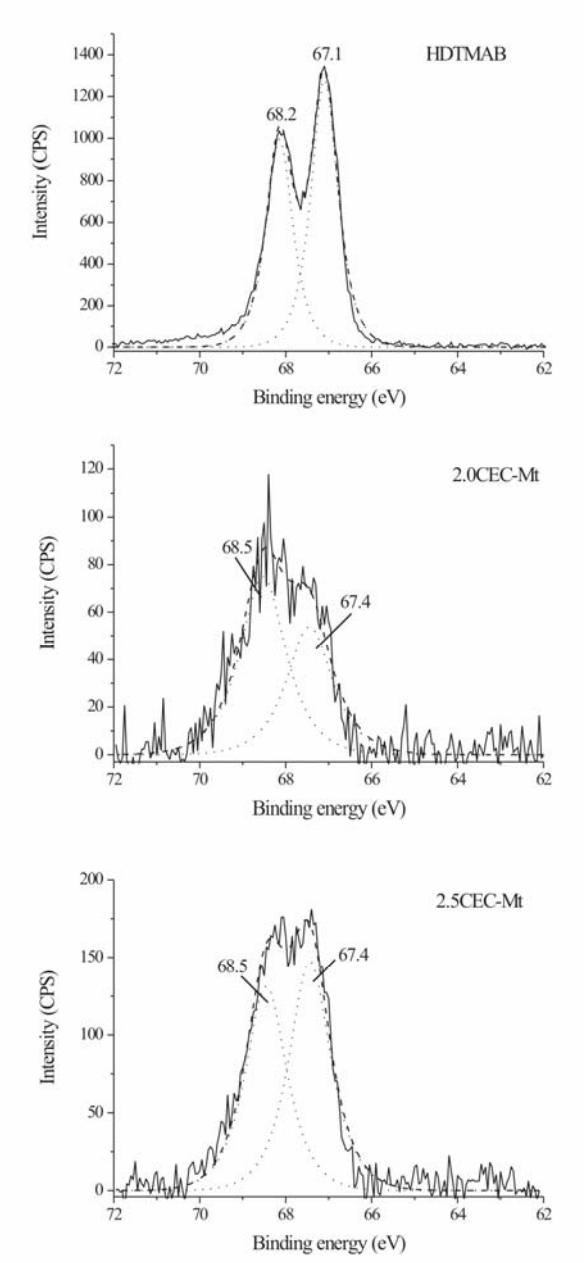

Figure 6 Br 3d high resolution XPS spectra of HDTMAB, 2.0CEC-Mt and 2.5CEC-Mt. solid line: experimental curve; dot line: deconvolution curve; dash line: fitting curve.

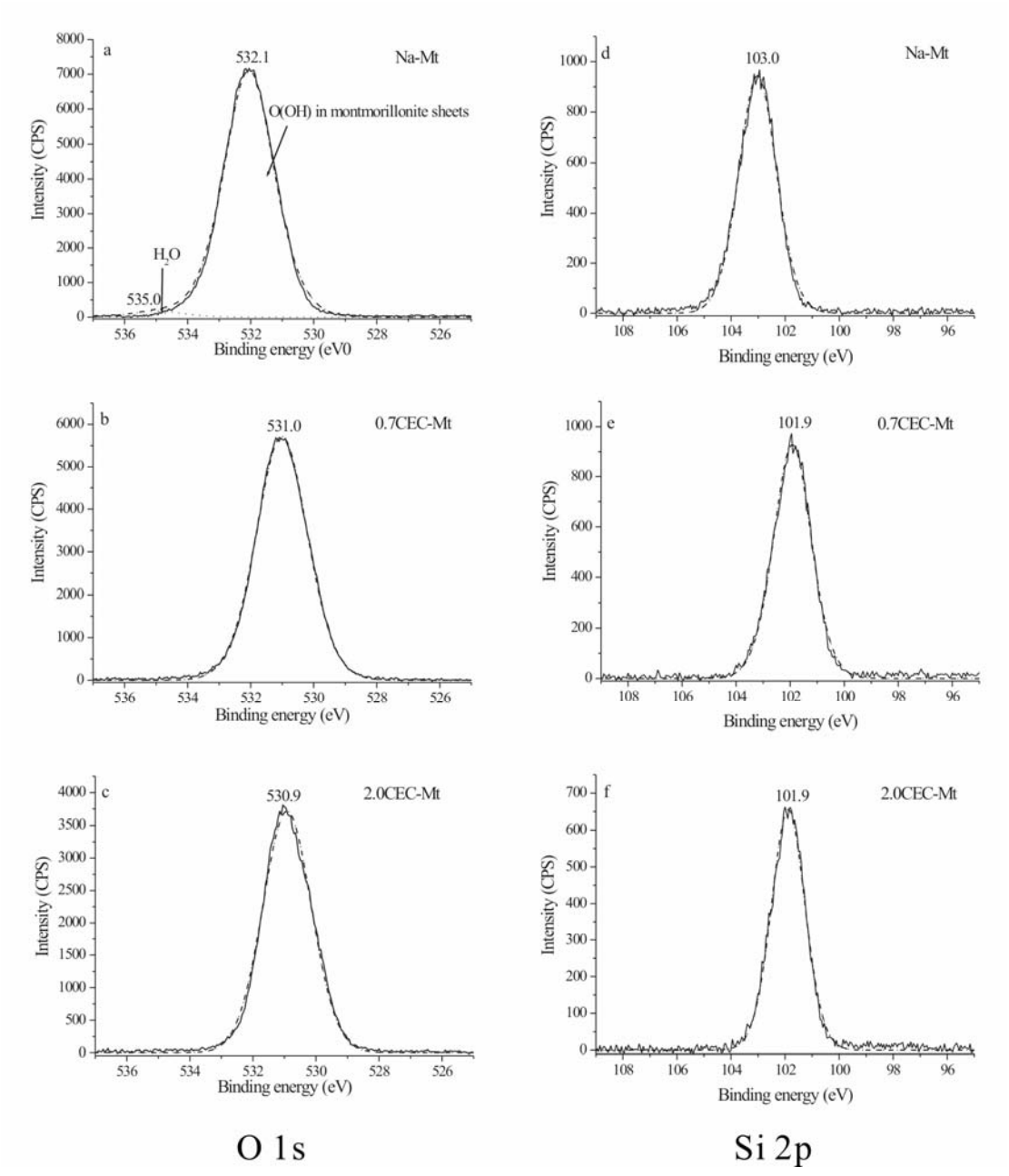

Figure 7 O 1s and Si 2p high resolution XPS spectra of Na-Mt and the representative organoclays. solid line: experimental curve; dot line: deconvolution curve; dash line: fitting curve.

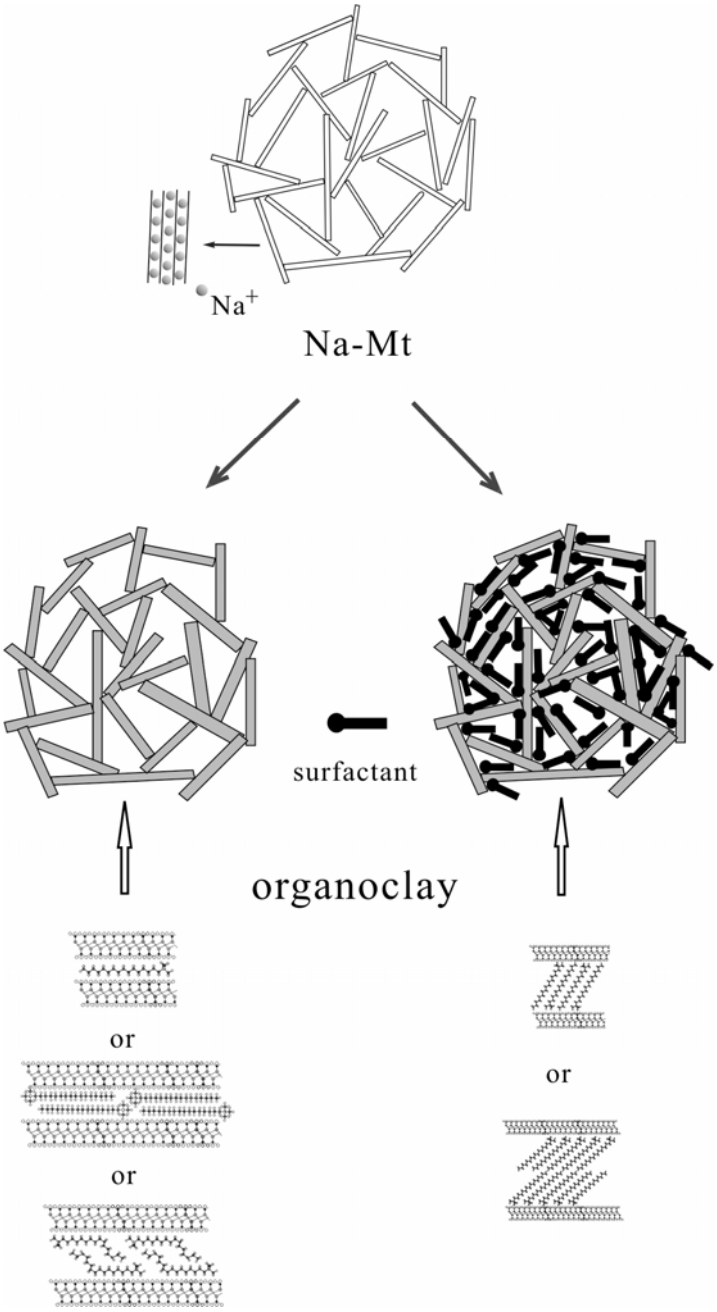

Figure 8 The schematics of Na-Mt and the resultant organoclays.